Quantitative near infra-red spectroscopy of massive stars

Stap, F.A.; Sana, H.; de Koter, A.

DOI
10.1088/1742-6596/328/1/012025
Publication date
2011
Document Version
Final published version
Published in
Journal of Physics. Conference Series

Quantitative near infra-red spectroscopy of massive stars

2011 J. Phys.: Conf. Ser. 328 012025

(http://iopscience.iop.org/1742-6596/328/1/012025)

Journal of Physics: Conference Series **328** (2011) 012025 doi:10.1088/1742-6596/328/1/012025

Quantitative near infra-red spectroscopy of massive stars

F A Stap[1], H Sana[1] and A de Koter[1,2]

[1] Anton Pannekoek Institute, PO box 94249, 1098XH Amsterdam, Netherlands
[2] Astronomical Institute, Utrecht University, Princetonplein 5, 3584CC Utrecht, Netherlands

E-mail: arjenstap@gmail.com

Abstract. Interest in near infra-red spectroscopy of massive stars has increased dramatically over the last decades, as it offers the possibility to analyze stars embedded in dusty star forming regions and near the Galactic center. We present an analysis of both high resolution optical and, separately, high resolution VLT/CRIRES near-IR spectra in the J, H, K and L-band of nearby dwarf O-type stars. Applying a genetic fitting algorithm approach using state-of-the-art FASTWIND non-LTE atmospheres, we present a comparison of the stellar and wind properties as derived from these two spectral regimes. In this approach we retrieve the effective temperature to within a sub-type and the surface gravity to within 0.2 dex, but find a discrepancy in the mass-loss rates of 0.2 up to 1.0 dex. We find that He II 1012 nm and Brackett-α lines do not yield consistent mass-loss estimates, the former producing much lower values than Hα, while Brackett-α and Hα are consistent.

1. Introduction

The Gaia space mission aims at obtaining phase space information of about one billion stars throughout our galaxy, amounting to roughly 1 percent of the Galactic stellar population [1]. Though of this grand total only a minor fraction will be of spectral type O, one may anticipate the discovery of massive, young stellar clusters similar to the 30 Doradus cluster in the Large Magellanic Cloud [2], each containing up to hundreds of O-type stars [3]. Their study will allow for an unprecedented view of the recent star forming activity of the Milky Way, and provide valuable information for the calibration of stellar population synthesis models.

Gaia spectrophotometry over the spectral range 3300–11500 Å and medium-resolution spectroscopy in the wavelength interval 8470–8740 Å will allow for a first characterization of the observed O stars [4], however, supplementary data is needed in order to derive robust stellar and stellar wind properties [5]. Fortunately, the Gaia-ESO Survey will provide optical spectra for a sub-set of about 1500 early-type stars (see Blomme, this Volume).

It will be clear that what is needed to accomplish this characterization are automated fitting techniques to perform quantitative spectral analysis. For the near-IR, so far an automated technique has been lacking. Clearly such a method would be most welcome as it allows to study early-type stars located in or near dusty star forming regions or seen over large distances along lines-of-sight through the Galactic plane, as at near-IR wavelengths the extinction caused by this material is substantially less than in the optical.

The characterization of O-type stars on the basis of their near-IR spectra started out with the compilation of spectral atlases [6–9] and rough classification schemes, mostly using

a morphological approach [6, 7]. However, Hanson et al. [9] conclude that to determine the effective temperature and surface gravity, profile fits with atmospheric model codes are necessary, stressing that, with the lack of spectroscopic standards for these spectral types, near-IR observations of known O- and B-type stars are needed to properly calibrate the near-IR properties of massive stars.

The first truly near-IR quantitative spectroscopic analysis, employing state-of-the-art FASTWIND (FW) model atmospheres [10] was performed by Repolust et al. [11]. These authors used intermediate resolution observations of 25 known OB stars, fitting the profiles of the seven strongest hydrogen and helium lines in the H- and K-band. Comparing their results to optical analysis, they find good agreement of the effective temperatures $T_{\rm eff}$ (to within 5%), gravities $\log g$ (to within 0.1 dex) and mass-loss rates $\dot{M}$ (to within 0.2 dex).

Here we present new high resolution ($R \sim 50\,000$) data of O dwarf standards, obtained with VLT/CRIRES [12], covering not only H and K, but also the J and L-band. For the first time, we employ an automated fitting technique, based on genetic algorithms [13], to derive stellar and stellar wind properties from these near-IR diagnostics, following [11] by using the non-local thermodynamic equilibrium, line blanketed, outflowing stellar atmosphere code FW. By applying the same analysis technique to optical spectra, we are able to assess the consistency of optical and near-IR analysis, confirming the findings of [11] for $T_{\rm eff}$ and g, but finding considerable discrepancies in the derived mass-loss rate.

2. Observations

The sample of targets is composed of bright dwarf stars that span the range of spectral sub-types. Although non-peculiar, non-multiple systems are preferred, the single-lined binary 15 Mon is also included. The targets HD 93250 and HD 54662 are proved to be binaries during the course of the project. We first briefly discuss the near-IR and optical data.

2.1. Near-IR spectra

The targets are observed with the CRyogenic high-resolution Infra-Red Echelle Spectrograph (CRIRES) mounted on the Very Large Telescope (VLT) at the ESO Paranal observatory (Chile), between December 2007 and February 2008. CRIRES provides observations between 1 to 5 μm with a resolving power of up to 10^5. The resolving power obtained in our data is 50 000 and is obtained with a slit width of $0.4''$. Spatial resolution and signal to noise ratio (SNR) are improved upon by the use of adaptive optics. The targets are observed in 18 different wavelength settings, chosen to cover important hydrogen and helium lines in the J-, H-, K- and L-band.

All the CRIRES observations are stacked, flat-fielded, corrected for dark, bias and detector linearity and wavelength calibrated using the ESO CRIRES pipeline [14]. A weighted map is used to optimize the extraction of the 1-D spectrum from the observation. Data suffering from the odd-even effect [15], as well as ghosts and bad pixels, are removed. Observations of telluric standards are used to divide out the atmospheric absorption lines in the spectra. In some cases, normalization of the spectra is done by fitting a second order polynomial to the continuum. The resulting SNR is mostly between 100 and 130, and as low as 50 in the worst cases.

2.2. Optical spectra

The optical spectra observed with either the Ultraviolet & Visual Echelle Spectrograph (UVES) [16] or the Fiber-fed Extended Range Optical Spectrograph (FEROS) [17], provide high quality spectra covering most of the optical range. The data are reduced using the UVES pipeline [18] or an improved version of the FEROS pipeline [19]. Both the FEROS and UVES spectra have a typical SNR of $\sim$300.

3. Spectral fitting

The analyses are performed by fitting FW line-profiles to the observations, using a Genetic Algorithm (GA) to find the best-fit stellar and wind parameters. This method has been readily established in the optical [13]. In this section we shortly discuss the stellar atmosphere code and describe our automated fitting method. We also introduce the important diagnostics and shortly elaborate on how Stark broadening was treated.

3.1. Fastwind

The stellar atmosphere code FW is optimized to swiftly calculate high quality models of early-type stars with effective temperatures of over 8500 K[1]. Constructing a model takes only ∼15 minutes, allowing us to compute a large number of models within a reasonable amount of time, making it ideal for automated fitting methods. To reduce computational time, appropriate physical approximations are used for processes where high accuracy is not needed [10].

3.2. Fitting method

In a GA based approach, thousands of FW models are calculated per analysis by means of parallel computing. The GA first constructs a number of models, the first generation, of which the free parameters are randomly chosen in the explored parameter space. The fitness (F) of these models is then calculated from the reduced chi square of the fits to the observed line-profiles. The parameters, or 'genes', that belong to the best models are used as input for the next generation, making small changes to their values to allow for convergence. Mutation (i.e. the process of changing the parameters by large amounts) ensures that the full extent of the parameter space is investigated. As opposed to Mokiem et al. [13] we use equal weights for all evaluated line profiles in the analyses.

The free parameters in this approach are the effective temperature ($T_{\rm eff}$), surface gravity (g), mass-loss rate ($\dot{M}$), the helium abundance ($n_{\rm He}/n_{\rm H}$), micro-turbulence velocity (ξ_μ), projected rotational velocity ($v_{\rm rot}\sin i$) and β, an empirical measure of the rate of acceleration of the flow as defined by a β-type velocity law.

B- and V-band photometry are taken from the SIMBAD Astronomical Database. We adopt the standard total to selective extinction value $R_{\rm V} = 3.1$, except for HD 93250 where we use $R_{\rm V} = 3.5$ [20]. Distances and absolute V-band magnitude $M_{\rm V}$ are listed in Table 1. Per model the effective temperature and $M_{\rm V}$ are used to derive the radius. From the radius and the surface gravity the mass and the surface escape velocity are derived. The terminal velocity of the flow is assumed to be $v_\infty = 2.6\ v_{\rm esc}$ [21]. Since, in this approach, we are unable to derive β for the dwarfs, we have set it equal to 0.8 in line with theoretical expectation [22]. We have assumed a solar metallicity [23]. No clumping has been included in the FW models.

3.3. Diagnostics

Fifteen and 18 hydrogen and helium profiles have been fitted in the optical and near-IR, respectively. As an example, Fig. 1 displays the CRIRES spectrum of 15 Mon together with its best-fit model. For constraining the effective temperature the GA mostly relies on the ratios of neutral and once ionized helium lines. In the near-IR the analysis mostly relies on He II 1691 nm, He I 1700 nm and He I 1031 nm. In the optical, temperature constraints are mainly provided by the He I λ4471 and He II λ4541. The gravity is constrained by the shapes of the hydrogen profiles that are not strongly affected by mass-loss: Paschen-δ and γ and Brackett-10, 11 and 12 in the near-IR and Balmer series lines in the optical. Strong diagnostic lines for the mass-loss rate are, in the near-IR, He II 1012 nm, Brackett-α and γ and, in the optical, Hα and He II λ4686.

[1] The code assumes that hydrogen remains fairly ionized and is not intended for stellar atmospheres that are sufficiently 'cool' for molecules to form and/or convection to set in.

Table 1. Properties of the program stars. The intrinsic color $(B-V)_0$ is taken from Martins et al. [24]. Column 6 lists the references for the adopted distance.

Object	V	$(B-V)_{\rm obs}$	$(B-V)_0$	Distance	Ref.	$M_{\rm V}$
HD 93250	8.25	+0.16	−0.28	2.5 kpc	[25]	-5.3^a
HD 46150	6.75	+0.12	−0.28	1.45 kpc	[26]	−5.3
HD 54662	6.68	−0.02	−0.27	1.3 kpc	[27]	-4.7^a
15 Mon	4.64	−0.24	−0.27	0.66 kpc	[26]	−4.6
HD 73882	7.27	+0.31	−0.27	1.15 kpc	[28]	−4.8

[a] Magnitudes are corrected for the presence of an unresolved companion (Sects. 4.1 and 4.3).

3.4. Stark broadening

Atmosphere codes depend on atomic data, for which accurate values are not always available. Of particular consequence for the near-IR spectral range is the absence of Stark broadening profiles. Stark broadening describes the constant perturbation of energy levels by the external electric fields of ions, electrons and atomic dipoles, resulting in broadening of the profiles. For hydrogen lines, even at low electron densities, the effect is of the same order of Doppler broadening [29] and thus needs to be taken into account. However, calculating the resultant broadening is computationally expensive and not yet carried out for many transitions. In the current version of FW, profiles that describe this broadening are included for most of the useful hydrogen and helium transitions in the optical but are mostly lacking for the near-IR transitions. For the hydrogenic transitions, we have approximated the effects of Stark broadening using Griem's approximation [29]. For most neutral helium transitions the Stark broadening is approximated using tabulated values for a Lorentz and Doppler profile.

4. Results

In this section we discuss the results of the GA analyses for every target. We briefly mention those lines that are not completely reproduced in the analysis. These discrepancies may arise due to the possible binarity of the targets, blends with transitions which we do not consider (such as the N III λ4200 transition that may be present in the He I λ4200 profile [13]) or missing physics in the atmosphere model (such as clumping, which may explain the difficulties in modelling, for example, the core of Brackett-γ [11]). Table 2 summarizes the results and Fig. 2 shows a comparison between effective temperatures, surface gravities and mass-loss rates obtained in the near-IR and the optical analyses.

4.1. HD 93250

HD 93250 has been selected because it is the brightest early O-type dwarf in the near-IR. Still, the target is not bright enough in the L-band and we therefore have no observation of the Brackett-α profile. Recent interferometric observations [30] confirm earlier indications of the target being a binary [31, 32]. The K-band luminosity ratio suggests a mass ratio close to unity and thus two very similar spectral components. Since the binary is not spatially resolved in our observations, we correct our photometry so that the GA adopts an appropriate radius for the FW models.

Both the near-IR and optical analysis reproduce the observations well with the exception of Brackett-γ and the effective temperature sensitive He I λ4471 and He II λ4541 lines. The error estimates on the effective temperature are large because of the near absence of neutral helium lines. Recently, HD 93250 (supposedly an O3 V star) has been re-classified as an O4 III star [33].

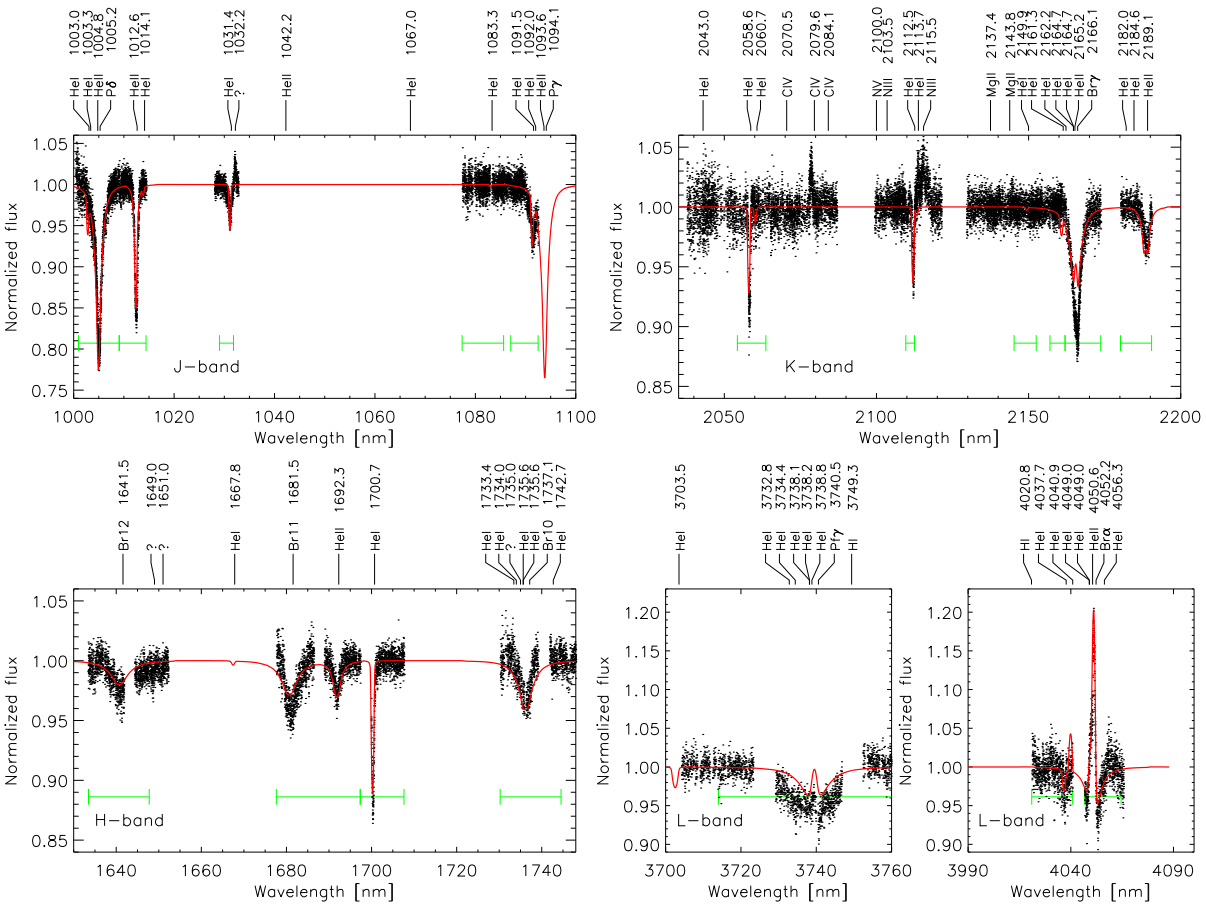

Figure 1. The spectra of 15 Mon over-plotted with the best fitting FW model in red. The green horizontal bars indicate the fitted spectral regions.

The surface gravity we obtain from the optical analysis is in better agreement with a giant [34]. The error-bars of the near-IR analysis allow for both luminosity classes.

4.2. HD 46150

HD 46150 is a mid-O star. Except for Brackett-10, Brackett-γ and Pfund-γ the near-IR analysis reproduces the observations to within the SNR. The optical analysis shows a very clean fit, except perhaps for the He II λ6683 profile. In the near-IR the temperature is not constrained. This is because the important He I 1700 nm line could not be retrieved from the near-IR data. As a consequence there is only a faint neutral Helium line to provide the temperature constraint.

4.3. HD 54662

HD 54662 is a long period binary with $P = 557.8$ days and a likely flux ratio of $F_{\rm sec} \sim 0.51\ F_{\rm prim}$ [35]. We use this flux ratio to correct the absolute visual magnitude for the companion.

All the synthetic profiles of the near-IR analysis agree to within the SNR of the observations, except for He II 1012 nm which is too weak. Nonetheless, the synthetic profiles of Brackett-γ, He II 2189 nm and Pfund-γ show structures that do not appear to be present in the observations. The optical analysis shows a number of synthetic profiles that neither agree with the observations. In general, the synthetic profiles are broader than the observed ones. The Balmer-ϵ line strength is slightly too large, while He I λ4541 and He II λ4686 are underestimated.

Table 2. Overview of the results from the optical and near-IR analyses. The spectral sub-type (Column 3) is obtained from the effective temperature using the calibration of Martins et al. [34].

Object	Spect. region	Spect. type	$T_{\rm eff}$ [K]	$\log g$ [cm s^{-2}]	$\log \dot{M}$ [$M_\odot$yr^{-1}]	$n_{\rm He}/n_{\rm H}$	$v_{\rm rot} \sin i$ [km s^{-1}]
HD 93250	IR	O3 V	$43900^{+\cdots}_{-1900}$	$3.84^{+0.11}_{-0.10}$	$-6.75^{+0.35}_{-\cdots}$	$0.07^{+0.04}_{-\cdots}$	134^{+52}_{-46}
	optical	O3 V	44200^{+1050}_{-1150}	$3.69^{+0.05}_{-0.05}$	$-5.75^{+0.05}_{-0.05}$	$0.07^{+0.01}_{-0.01}$	138^{+10}_{-10}
HD 46150	IR	O4 V	$42450^{+\cdots}_{-\cdots}$	$3.70^{+0.18}_{-\cdots}$	$-6.90^{+0.50}_{-\cdots}$	$0.06^{+0.04}_{-\cdots}$	152^{+46}_{-40}
	optical	O5 V	41500^{+600}_{-550}	$3.84^{+0.06}_{-0.05}$	$-5.95^{+0.05}_{-0.05}$	$0.07^{+0.01}_{-0.01}$	120^{+10}_{-10}
HD 54662	IR	O6 V	38850^{+2800}_{-1850}	$3.94^{+0.33}_{-0.23}$	$-6.65^{+0.25}_{-0.65}$	$0.07^{+0.07}_{-\cdots}$	76^{+50}_{-16}
	optical	O7 V	37300^{+1100}_{-300}	$3.73^{+0.12}_{-0.05}$	$-6.45^{+0.10}_{-0.30}$	$0.08^{+0.02}_{-0.02}$	126^{+14}_{-16}
15 Mon	IR	O6 V	38000^{+300}_{-600}	$3.92^{+0.05}_{-0.05}$	$-6.95^{+0.30}_{-0.05}$	$0.09^{+0.02}_{-0.03}$	78^{+20}_{-18}
	optical	O6 V	38350^{+300}_{-500}	$3.94^{+0.05}_{-0.05}$	$-6.25^{+0.05}_{-0.05}$	$0.07^{+0.01}_{-0.01}$	80^{+10}_{-10}
HD 73882	IR	O7 V	$36750^{+\cdots}_{-\cdots}$	$3.32^{+0.22}_{-0.26}$	$-6.20^{+0.15}_{-0.35}$	$0.06^{+0.20}_{-\cdots}$	222^{+146}_{-108}
	optical	O8.5 V	33750^{+1600}_{-300}	$3.43^{+0.14}_{-0.05}$	$-6.55^{+0.20}_{-0.20}$	$0.09^{+0.02}_{-0.03}$	202^{+10}_{-16}

The helium blend He II λ6683 does not show the correct shape and the synthetic neutral helium lines do not show equally sharp line-centers as the observations. These discrepancies may be explained by the binarity of the target.

4.4. 15 Mon

15 Mon is both an astrometric and a spectroscopic, long-period ($P \sim 25$ yr) binary with a separation of about two arc-seconds [36]. In the acquisition images of CRIRES, the companion is positioned just outside the slit. We are uncertain whether we have observed a composite spectrum in the optical.

The optical and near-IR analysis reproduce the observed spectra very well, see Fig. 1. Minor discrepancies are found in the optical, where the line-centers are slightly too weak in the synthetic spectra. In the near-IR, where the SNR is lower, all the synthetic profiles are within the noise, except for He I 4040 nm and the cores of Brackett-γ and Pfund-γ.

4.5. HD 73882

HD 73882 is the ionizing star of the H II region RCW 27 [28]. The absolute visual magnitude that is derived from the photometry and distance is too luminous for an O8.5 dwarf and is better suited for an O6.5 V, or, if we have underestimated the extinction, a late O-type giant. Cardelli et al. [37] find that HD 73882 is a highly reddened star with a R_V of 3.39.

The SNR in the near-IR is significantly lower than for our other targets. The best model retrieved in the near-IR analysis is a poor fit, both in terms of fitness and a by eye evaluation. The analysis in the optical has difficulties converging and also yields a poor fit in terms of fitness. A plausible explanation for these difficulties might be that we have used an erroneous absolute visual magnitude due to our assumption $R_{\rm v} = 3.1$. This will be investigated in the near future.

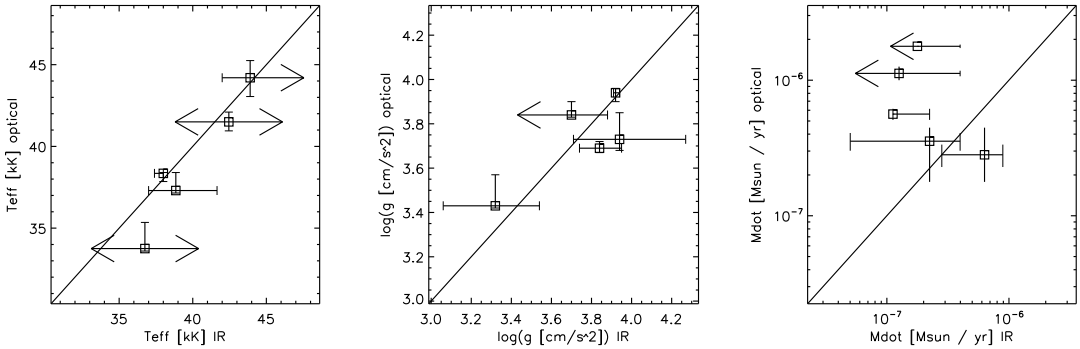

Figure 2. Comparison of the best fit parameters ($T_{\rm eff}$, $\log g$, $\dot{M}$) obtained for the near-IR and optical. Error-bars indicate the estimated errors, while left/right arrows indicate upper/lower limits.

5. Discussion & Conclusion

We have presented first results of detailed spectral fitting of hydrogen and helium profiles in the J, H, K and L-band of known, bright, O-type dwarfs. A comparison with our optical analysis shows agreement in effective temperature to within a sub-type[2]. The surface gravity agrees to within 0.2 dex. For the mass-loss rates we find a discrepancy of 0.2 up to 1.0 dex. We find that, for the investigated spectral types, the He II 1012 nm transition is more sensitive to the mass-loss rate than Brackett-α. The mass-loss rate derived from Brackett-α is actually in good agreement with the optical results (recall that we have no L-band observation of HD 93250). However, much lower mass-loss rates are found when using the He II 1012 nm profile. We are currently investigating whether differential clumping properties in the line forming regions may explain this inconsistency.

We plan to extend our analysis to giant and supergiants to fully cover the O star parameter range. This will allow us to further explore the discrepancy in the retrieved mass-loss rates. We conclude that the first GA based automated fitting comparison between optical and near-IR spectroscopic analysis of dwarf O stars yields very promising results, especially for the effective temperature and surface gravity.

References

[1] Perryman M A C, de Boer K S, Gilmore G, Høg E, Lattanzi M G, Lindegren L, Luri X, Mignard F, Pace O and de Zeeuw P T 2001 *A&A* **369** 339–63

[2] Evans C J *et al* 2011 *A&A* **530** A108

[3] Hanson M M and Popescu B 2008 *IAU Symposium* vol 250 ed F Bresolin, P A Crowther, & J Puls pp 307–12

[4] Bouret J C, Lanz T, Frémat Y, Martins F, Lefever K, Blomme R, Martayan C, Neiner C, Quinet P and Zorec J 2008 *Rev. Mexicana Astron. Astrofis. Conf. Ser.* vol 33 pp 50–50

[5] Blomme R, Frémat Y, Lobel A and Martayan C 2011 *EAS Publications Ser.* vol 45 pp 373–76

[6] Hanson M M, Conti P S and Rieke M J 1996 *ApJS* **107** 281–311

[7] Conti P S and Howarth I D 1999 *MNRAS* **302** 145–51

[2] With the exception of HD 73882. However, we note that the absolute visual magnitude we used for this star indicates that it is over-luminous.

[8] Lenorzer A, Vandenbussche B, Morris P, de Koter A, Geballe T R, Waters L B F M, Hony S and Kaper L 2002 *A&A* **384** 473–90

[9] Hanson M M, Kudritzki R P, Kenworthy M A, Puls J and Tokunaga A T 2005 *ApJS* **161** 154–70

[10] Puls J, Urbaneja M A, Venero R, Repolust T, Springmann U, Jokuthy A and Mokiem M R 2005 *A&A* **435** 669–98

[11] Repolust T, Puls J, Hanson M M, Kudritzki R P and Mokiem M R 2005 *A&A* **440** 261–86

[12] Kaeufl H-U *et al* 2004 *SPIE Conf. Ser.* vol 5492 ed A F M Moorwood & M Iye pp 1218–27

[13] Mokiem M R, de Koter A, Puls J, Herrero A, Najarro F and Villamariz M R 2005 *A&A* **441** 711–33

[14] Jung Y and Bristow P 2008 *2007 ESO Instrument Calibration Workshop* ed A Kaufer & F Kerber pp 225–8

[15] Smoker J 2011 *CRIRES User Manual v88.4* European Southern Observatory

[16] Dekker H, D'Odorico S, Kaufer A, Delabre B and Kotzlowski H 2000 *SPIE Conf. Ser.* vol 4008 ed M Iye & A F Moorwood pp 534–45

[17] Kaufer A, Stahl O, Tubbesing S, Nørregaard P, Avila G, Francois P, Pasquini L and Pizzella A 1999 *The Messenger* **95** 8–12

[18] Sana H 2009 *A&A* **501** 291–5

[19] Sana H, Hensberge H, Rauw G and Gosset E 2003 *A&A* **405** 1063–74

[20] Carraro G, Romaniello M, Ventura P and Patat F 2004 *A&A* **418** 525–37

[21] Lamers H J G L M, Snow T P and Lindholm D M 1995 *ApJ* **455** 269–85

[22] Muijres L E 2011 Ph.D. thesis Univ. Amsterdam

[23] Asplund M, Grevesse N and Sauval A J 2005 *Cosmic Abundances as Records of Stellar Evolution and Nucleosynthesis* (*PASP Conf. Ser.* vol 336) ed T G Barnes III & F N Bash pp 25–38

[24] Martins F and Plez B 2006 *A&A* **457** 637–44

[25] Rauw G, Nazé Y, Fernández Lajús E, Lanotte A A, Solivella G R, Sana H and Gosset E 2009 *MNRAS* **398** 1582–92

[26] Kharchenko N V, Piskunov A E, Röser S, Schilbach E and Scholz R D 2005 *A&A* **438** 1163–73

[27] Megier A, Strobel A, Galazutdinov G A and Krełowski J 2009 *A&A* **507** 833–40

[28] Urquhart J S, Morgan L K and Thompson M A 2009 *A&A* **497** 789–804

[29] Griem H R 1960 *ApJ* **132** 883–93

[30] Sana H, Le Bouquin J B, De Becker M, Berger J P, de Koter A and Mérand A 2011 *ApJL* **740** L43–8

[31] Leitherer C, Chapman J M and Koribalski B 1995 *ApJ* **450** 289–301

[32] Antokhin I I, Rauw G, Vreux J M, van der Hucht K A and Brown J C 2008 *A&A* **477** 593–609

[33] Walborn N R, Sota A, Maíz Apellániz J, Alfaro E J, Morrell N I, Barbá R H, Arias J I and Gamen R C 2010 *ApJL* **711** L143–7

[34] Martins F, Schaerer D and Hillier D J 2005 *A&A* **436** 1049–65

[35] Boyajian T S, Gies D R, Dunn J P, Farrington C D, Grundstrom E D, Huang W, McSwain M V, Williams S J, Wingert D W, Fullerton A W and Bolton C T 2007 *ApJ* **664** 1121–9

[36] Gies D R, Mason B D, Hartkopf W I, McAlister H A, Frazin R A, Hahula M E, Penny L R, Thaller M L, Fullerton A W and Shara M M 1993 *AJ* **106** 2072–80

[37] Cardelli J A, Clayton G C and Mathis J S 1989 *ApJ* **345** 245–56